Journal of
Composites Science

IMPACT FACTOR 3.3

CITESCORE 4.5

Article

Multiscale Toughening of Composites with Carbon Nanotubes—Continuous Multiscale Reinforcement New Concept

Monssef Drissi-Habti, Yassine El Assami and Venkadesh Raman

Special Issue
Vibration-based Energy Harvesting Techniques via Smart Materials and Structures

Edited by
Dr. S.K. Lai and Prof. Dr. Songye Zhu

MDPI

https://doi.org/10.3390/jcs5050135

Journal of
Composites Science

MDPI

Article

Multiscale Toughening of Composites with Carbon Nanotubes—Continuous Multiscale Reinforcement New Concept

Monssef Drissi-Habti *, Yassine El Assami and Venkadesh Raman

COSYS-LISIS, Université Gustave Eiffel, IFSTTAR, F-77447 Marne La Vallée, France; yassine.elassami@ifsttar.fr (Y.E.A.); venkadesh.raman@ifsttar.fr (V.R.)
* Correspondence: monssef.drissi-habti@univ-eiffel.fr

Abstract: Strengthening composite structures for advanced industries such as offshore wind generation is a real issue. Due to the huge dimensions expected for next generation wind-blades, composites based on glass fibers can no longer be used due to the lack of stiffness, whereas composites based on carbon fibers are expensive. Therefore, switching to alternative structural solutions is highly needed. This might be achieved by appropriate use of carbon nanotubes (CNTs) either as fillers of epoxy matrices, especially in inter-plies, or as fillers of epoxy glues used in structural bonding joints. As an example, trailing edges of offshore wind-blades are addressed in the current article, where monolithic bonding holds together the two structural halves and where the risk of sudden and brittle separation of edges while wind-turbines are in service is quite high. This can lead to tedious and very expensive maintenance, especially when keeping in mind the huge dimensions of new generation wind turbine blades that exceed lengths of 100 m. Bond joints and composites inter-plies of the final CNT-reinforced structures will exhibit stiffness and toughness high enough to face the severe offshore environment. In this article, multiscale Finite Element (FE) modeling is carried out to evaluate mechanical properties following the addition of CNTs. To achieve an optimal reinforcement, the effect of inclination of CNTs vs. mechanical loading axis is studied. Two innovations are suggested through this numerical study: The first consists of using homogenization in order to evaluate the effects of CNT reinforcement macroscopically. The second innovation lies in this forward-looking idea to envisage how we can benefit from CNTs in continuous fiber composites, as part of a deep theoretical rethinking of the reinforcement mechanisms operating at different scales and their triggering kinetics. The presented work is purely numerical and should be viewed as a "scenario" of structural composite materials of the future, which can be used both in the offshore industry and in other advanced industries. More broadly and through what is proposed, we humbly wish to stimulate scientific discussions about how we can better improve the performances of structural composite materials.

Keywords: finite element; carbon nanotubes; smart composites; homogenization; offshore; wind-blade; energy generation; continuous multiscale reinforcement concept

Citation: Drissi-Habti, M.; El Assami, Y.; Raman, V. Multiscale Toughening of Composites with Carbon Nanotubes—Continuous Multiscale Reinforcement New Concept. *J. Compos. Sci.* **2021**, *5*, 135. https://doi.org/10.3390/jcs5050135

Academic Editors: S. K. Lai and Songye Zhu

Received: 6 April 2021
Accepted: 12 May 2021
Published: 18 May 2021

1. Introduction

To significantly improve the performance of smart composites [1–3], the current article work assesses the benefits of CNTs as fillers to epoxy resin by way of a numerical multiscale method simulation. The cases that are under focus are (Figure 1):

(1) Increasing the stiffness of inter-plies by CNT-reinforced resin. Moreover, if CNT orientation can be optimized, through reinforcement mechanisms (crack-bridging and pull-out), delamination strength will be enhanced.
(2) Reinforcement of composite bonding joints by CNT-reinforced resin, which will result in higher bonding strength, and thus improve joints' toughness.

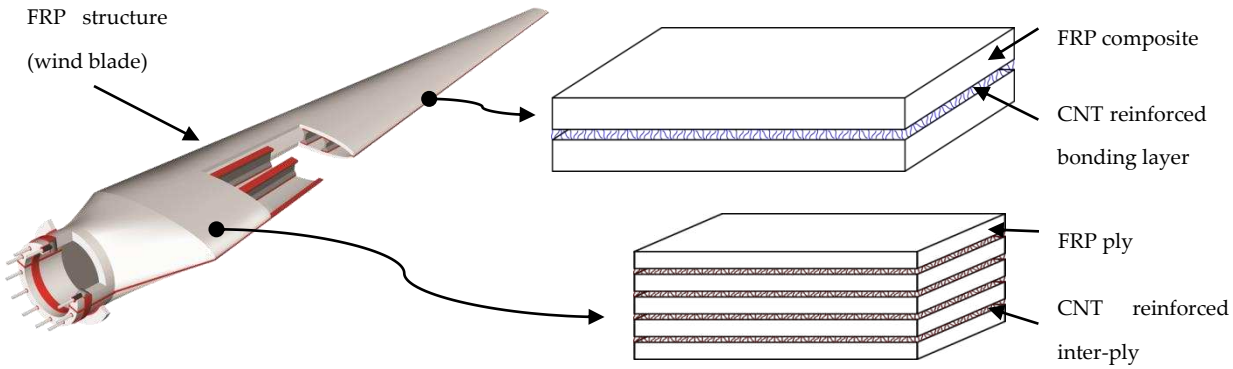

Figure 1. The bonding joints and the composite inter-ply areas of large wind turbine blades are the areas where a matrix reinforced by CNTs is expected to increase the toughness.

In the current article, the effect of CNT orientation vs. the loading direction is studied in a way to show proof of concept of toughness improvement at the laboratory scale, hoping that mastering inclination techniques can be achieved soon, industrially. Various loading configurations have been studied numerically at the nanoscale. The model that is suggested is based on an energy approach. Euler beam elements represent covalent carbon bonds. Chirality and functionalization have been studied through atomic simulation, where the interface between the CNT and matrices is governed by Van der Waals forces.

2. Atomic Structure of CNTs

CNTs exhibit exceptional mechanical and physical properties. Amounts ranging between wt. 0.4% and 1% are efficient enough to reinforce matrices significantly [4–7] while keeping the final structural weight unchanged [8–14]. A single-walled CNT is depicted in Figure 2. Chirality (chirality vector $\vec{C} = n\vec{a_1} + m\vec{a_2}$) governs mechanical properties (strength) as well as some other physical properties [6,15–17].

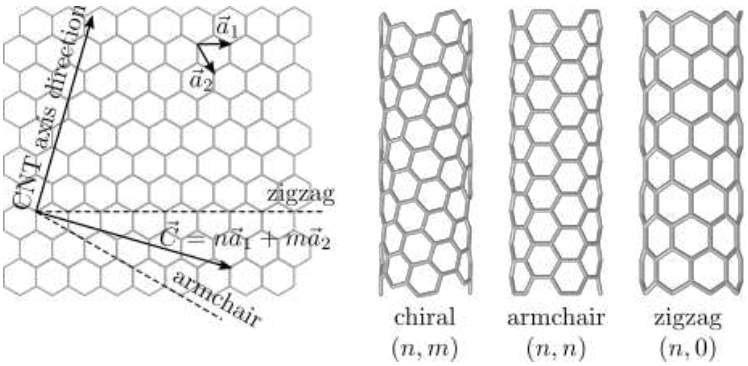

Figure 2. Illustration of CNT's chirality.

Chirality has an influence on CNT elastic properties, but its influence is more noticeable for strength, thermal and electrical properties [6,15–17].

3. Modeling CNTs and CNT–Matrix Interface

Given the nanosize of CNTs, their interactions with polymers have been studied using molecular dynamics in order to evaluate their mechanical behaviors [8,9,18–21], whereas continuum mechanics has been used to model polymers behavior. The issue of scale separation has been under focus for many years and led, for example, to the atomic-scale finite element method (AFEM), where some mechanisms such as post-buckling were described [19,22–24]. Another approach suggested modeling carbon bonding using a Euler Beam based space-frame [25–27]. Details about beam sections have been suggested by [28].

In the current article, molecular dynamics is used to study CNTs, an approach which is similar to the ones of [29,30]. It is well-established that functionalization is strongly enhancing CNT–polymer interface strength [31–33]. The influence of functionalization has been shown to be temperature-dependent [34] and that it increases, more specifically, fracture toughness [31].

FE has been used to model CNT–polymer interfaces. Beam-spring elements have been used by [21], where every CNT atom is bonded to matrix mesh nodes. Truss elements were used in a continuum model to model van der Waals bonding [20]. Discrete truss rods were also used by [27] and [29] to model van der Waals CNT–polymer interfaces and used the generalized displacement control method proposed by [35]. Functionalization by amino groups has been modeled by [36]. Another option that is based on a continuous layer, illustrating van der Waals forces, was also studied by [37] and a cohesive law was derived that takes into account various interactions. There are also various models that ease the modeling of van der Waals interactions within MW-CNTs [38].

In this article, FE has been used. Modeling CNTs at the atomic level make it possible to control their structures. It allows functionalization defects to be considered as well [36,39]. Based on previous works, the CNT–polymer interface has been modeled by a continuous layer [39–41], as is the case in our modeling. To evaluate CNT-reinforced matrix elastic behavior, a homogenization approach was used and the stiffness tensor made it possible to evaluate the mechanical behavior that emphasizes CNT reinforcement effects vs. the three loading directions. The first innovation brought by this work is the attempt to make a link between nanoscale modeling and macroscopic mechanical behavior through homogenization, knowing that CNT reinforcement becoming increasingly prevalent in various industries. The article presents a calculation that shows benefits of the use of CNTs to reinforce composites. These calculations can be used as a discussion basis of further articles that will address the same issues. The second innovation lies in this prospective idea where we tried to glimpse the industrial potential of the double reinforcement of polymer matrices with continuous fibers and also by carbon nanotubes. The objective is to consider a new concept of composites, which would enable all reinforcement scales (from nano to macro) to be fully engaged as soon as the material is subjected to mechanical stress.

4. Theory

As mentioned, current simulations use Beam theory to model carbon-carbon bonding; the polymer is a continuous material and a CNT–polymer interface is a layer governed by van der Waals interactions. The model considers a CNT weight fraction $f_w = 1\%$ ([10,17,32,42]). The estimation of the number of atoms in a given CNT is conducted through:

$$V_{\text{mat}} = \left(\frac{1}{f_w} - 1\right)\frac{n_C M_C}{\rho_{\text{mat}}} \tag{1}$$

where V_{mat} is the volume of the matrix of the nanocell, n_C is the number of carbon atoms in the CNT, M_C is the weight of a single carbon atom and ρ_{mat} is the matrix density.

The CNT is modeled by a free lattice, where carbon-carbon bonding is considered as a cylindrical beam of length, L, and radius, r:

$$\frac{EA}{L} = k_r \quad , \quad \frac{EI}{L} = k_\theta \quad , \quad \frac{GJ}{L} = k_\tau \tag{2}$$

E and G are the beam Young's and shear moduli, the section surface $A = \pi r^2$, $I = \frac{\pi r^4}{4}$ is the second moment and $J = \frac{\pi r^4}{2}$ is the polar moment. k_r, k_θ and k_τ are the force constants of stretching, bending and torsional resistance tabulated using molecular dynamics [9,20,43,44]. Note that Equation (2) and Figure 3 show the analogy between Beam theory and molecular dynamics [20,26,30]. The properties of the circular beam can be computed using:

$$r = 2\sqrt{\frac{k_\theta}{k_r}} \quad , \quad E = \frac{k_r^2 L}{4\pi k_\theta} \quad , \quad G = \frac{k_r^2 k_\tau L}{8\pi k_\theta^2} \tag{3}$$

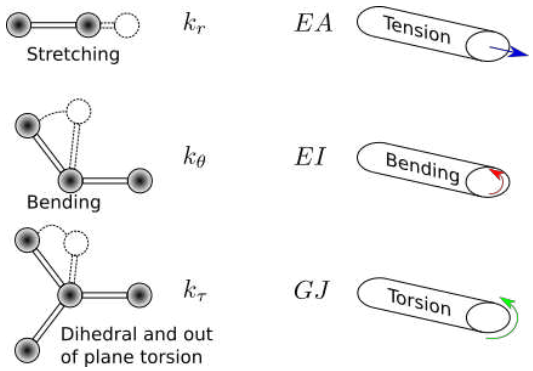

Figure 3. Molecular dynamics can illustrate atomic interactions.

$L = 0.1421$ nm is the length of the carbon-carbon bond [43]. Various bond forces constants are considered [28]. Using Equation (3), a Poisson's ratio higher than 0.5 was calculated [27,45,46]. The authors of [28], following [47], calculated a more accurate Poisson's ratio value that was adopted in the current article: $k_r = 786$ nN/nm, $k_\theta = 0.901$ nN nm/rad^2 and $\nu = 0.0344$. Young's modulus of the beam is $E = 7753$ GPa and $r = 0.0677$ nm. Knowing that CNT's diameter does not relate systematically to its thickness as shown by [47] and assuming the thickness is the same as one graphene sheet ($t = 0.34$ nm, [26,27]), CNT's Young's modulus E_{cnt}, is given by:

$$E_{\text{cnt}} = \frac{F}{2\pi R t} \frac{L_{\text{cnt}}}{\Delta L_{\text{cnt}}} \tag{4}$$

where F is the force applied to a CNT and $\Delta L_{\text{cnt}}/L_{\text{cnt}}$ its the elastic strain. The Young's modulus calculated is E_{cnt} is 1.18 TPa.

Carbon-carbon bonds were considered to have constant lengths and it was assumed that each carbon atom interacts in one unique point with the matrix (Figure 4b). Figure 4a shows a schematic of van der Waals forces that should bond the CNT and the matrix. To ease calculations, some simplifications were applied (Figure 4c). In this work, van der Waals forces' effective behavior is modeled with a continuous layer that is different from the polymer (Figure 4e).

Averaging CNT–matrix interactions allow the calculations of the forces and a cohesive behavior of the interface, which considers interacting particles densities and atomic potential constants can be tabulated from [37]:

$$\sigma_{\text{coh}} = 2\pi\rho_p\rho_c\varepsilon\sigma^2\left[\frac{\sigma^4}{(h+v)^4} - \frac{2\sigma^{10}}{5(h+v)^{10}}\right] \tag{5}$$

Equation (5) gives the cohesive stress σ_{coh} and the opening v of a graphene sheet interacting with a matrix (Figure 5). Note that the cohesive stress depends on the rolling effect of the graphene layer, though this can be neglected as shown by [37]. The law uses volume density, ρ_p, of polymer atoms, the surface density of C in the CNT, ρ_c, and the Lennard–Jones 6–12 potential constants ε and σ.

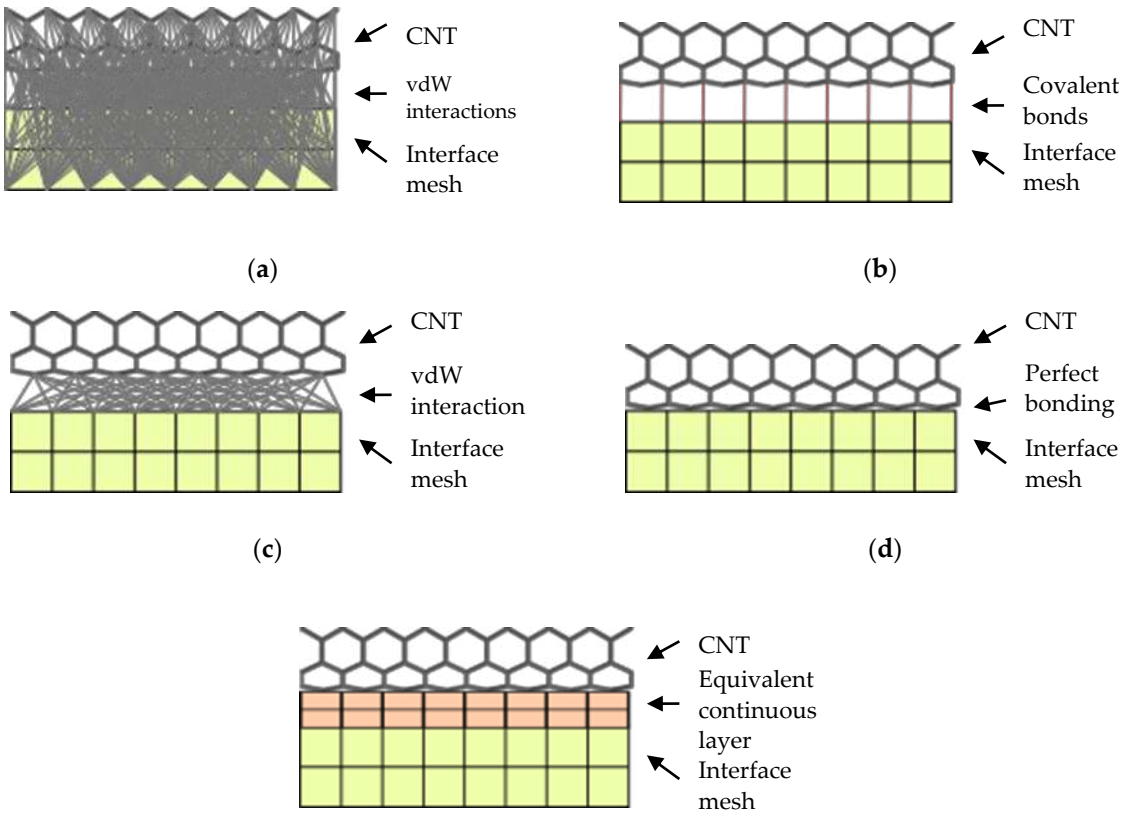

Figure 4. Interface modeling: (**a**) CNT and matrix show covalent bonding; (**b**) CNT and matrix have van der Waals bonding; (**c**) perfect bonding; (**d**) van der Waals bonding is achieved through a continuous layer, which is considered in the current article (**e**).

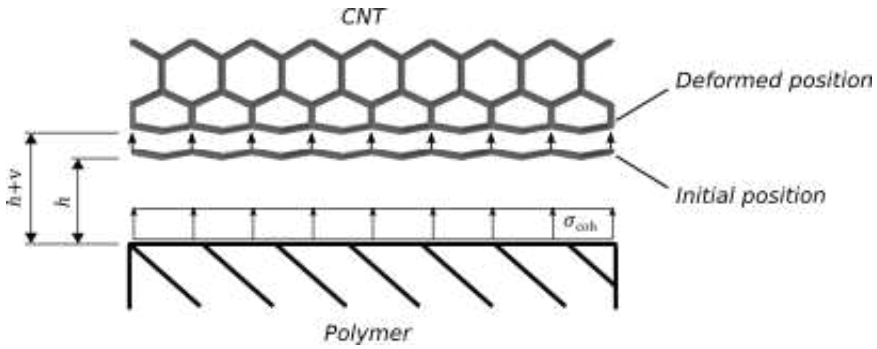

Figure 5. Van der Waals bonding between matrix and CNT.

The CNT and matrix equilibrium distance are given by $h = \left(\frac{2}{5}\right)^{\frac{1}{6}}\sigma$, knowing that the potential that yields the tensile stress is minimal. Using [4], the Young's modulus of the inlayer:

$$E_{\text{int}} = 30\left(\frac{2}{5}\right)^{\frac{1}{3}}\pi\rho_p\rho_c\varepsilon\sigma^2 \tag{6}$$

The interfacial maximum is met when $v = \sigma - h$ and is:

$$\sigma_{\text{coh}}^{\max} = \sigma_{\text{coh}}(\sigma - h) = \frac{6\pi}{5}\rho_p\rho_c\varepsilon\sigma^2 \tag{7}$$

For the calculations, we used the values that were detailed elsewhere [4,37]—i.e., $\sigma = 0.3825$ nm and $\varepsilon = 7.462 \times 10^{-4}$ nN · nm and $\rho_c = \frac{4}{3\sqrt{3}L^2} = 38.1$ nm^{-2}, ρ_p is 1174 kg/m^3, $\rho_p = 46.0$ nm^{-3} [4]. The cohesive stress can be derived in a way that allows the meshing through tetrahedral elements and a Poisson's ratio taken equal to the polymer is adopted, which makes it possible to consider shear [4,41,48].

5. Representative Volume Element (RVE)

To define the representative volume element (RVE), the following parameters have been used: Epon 862 [49,50], Young's modulus and Poisson's ratio were $E_{\text{mat}} = 2.92$ GPa and $\nu_{\text{mat}} = 0.4$, the tensile strength was 76 MPa and tetrahedra was considered for meshing [4] and finally the RVE was used to solve homogenization problem.

6. Homogenization

For homogenization simulations, CNT was assumed to be fully embedded inside the matrix and all boundary conditions were acting on its extremities (Figure 6).

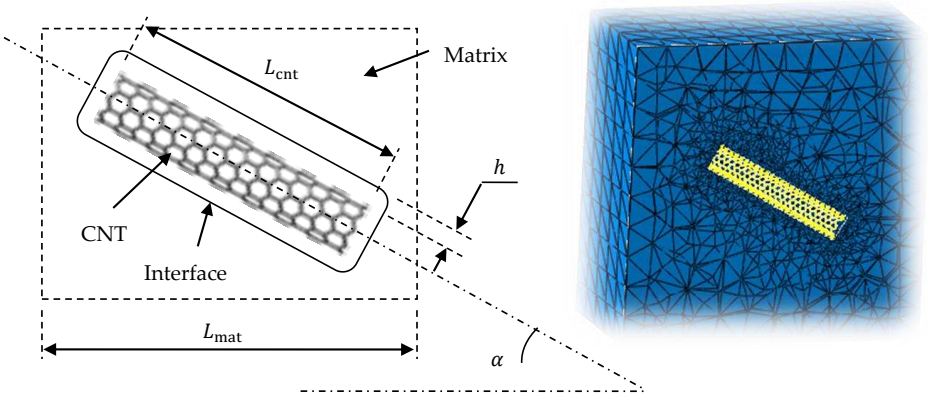

Figure 6. Details of FE modeling.

To tabulate macroscopic properties of the cell, various loading configurations were considered. Additionally, the effective behavior, macroscopic strain, $\overline{\varepsilon}$, and stress, $\overline{\sigma}$, must be calculated:

$$\begin{aligned} \overline{\sigma} &= \tfrac{1}{|\Omega|}\int_\Omega \sigma \, \mathrm{d}V \quad \text{(a)} \\ \overline{\varepsilon} &= \tfrac{1}{|\Omega|}\int_\Omega \varepsilon \, \mathrm{d}V \quad \text{(b)} \end{aligned} \tag{8}$$

Since the carbon nanotube is considered as the CNT and as a lattice, $\boldsymbol{\varepsilon}\,\mathrm{d}V$ and $\boldsymbol{\sigma}\,\mathrm{d}V$ are not defined throughout the RVE, Ω. To avoid this issue, the Gauss–Ostrogradsky theorem applies [51]:

$$\begin{aligned} \overline{\sigma} &= \tfrac{1}{|\Omega|}\int_{\partial\Omega} \boldsymbol{x} \otimes \boldsymbol{t} \, \mathrm{d}S \quad \text{(a)} \\ \overline{\varepsilon} &= \tfrac{1}{2|\Omega|}\int_{\partial\Omega} (\boldsymbol{n} \otimes \boldsymbol{u} + \boldsymbol{u} \otimes \boldsymbol{n}) \, \mathrm{d}S \quad \text{(b)} \end{aligned} \tag{9}$$

where $\boldsymbol{x}$ is the borders coordinate, $\partial\Omega$, $\boldsymbol{n}$ is the vector perpendicular to the surface, $\boldsymbol{t} = \sigma \cdot \boldsymbol{n}$ is the surface traction and $\boldsymbol{u}$ is the displacement of $\boldsymbol{x}$. The evaluation of macroscopic stress and strain can be achieved by acquiring $\boldsymbol{u}_i$, $\boldsymbol{n}_i$, $\boldsymbol{t}_i$ and $\mathrm{d}S_i$ for each element i on the outer surface. Macroscopic quantities of Equation (9) can be evaluated by:

$$\begin{aligned} \overline{\sigma} &\approx \tfrac{1}{|\Omega|}\sum_{i\in\partial\Omega} \boldsymbol{x}_i \otimes \boldsymbol{t}_i \, \mathrm{d}S_i \quad \text{(a)} \\ \overline{\varepsilon} &\approx \tfrac{1}{2|\Omega|}\left(\boldsymbol{\epsilon} + \boldsymbol{\epsilon}^{\mathrm{T}}\right) \text{ where } \boldsymbol{\epsilon} = \sum_{i\in\partial\Omega} \boldsymbol{n}_i \otimes \boldsymbol{u}_i \, \mathrm{d}S_i \quad \text{(b)} \end{aligned} \tag{10}$$

The macroscopic nanocomposite stiffness tensor, $\mathbb{C}$, as well as elastic properties as a function of CNT orientation can therefore be calculated using Equation (10).

7. Results

7.1. Influence of CNT Orientation

FE modeling allowed the visualization of the complete scenario of how the CNT is orientated (angle α) vs. loading axis acts in the RVE (Figures 6 and 7). Details have been given elsewhere [4,27,30,36]).

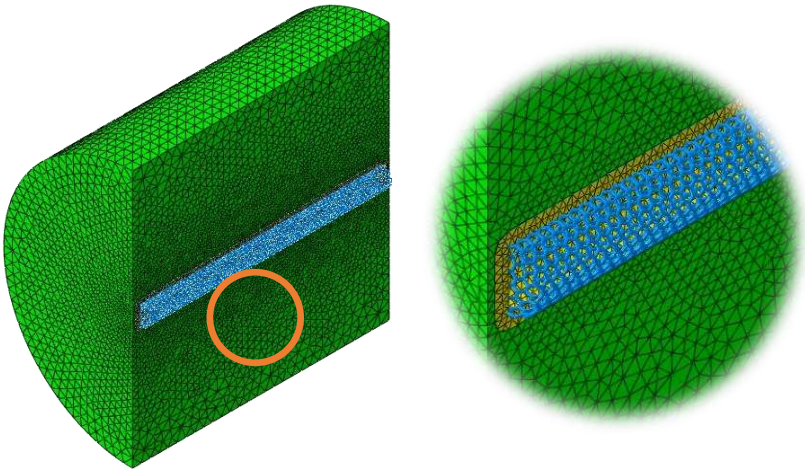

Figure 7. Models used for tension, compression and torsion simulations.

7.2. Tension and Compression

Tension and compression curves are depicted in Figure 8 for various orientations and compared to the curve of unreinforced matrix. Note that the highest benefit in reforcing with CNT is clearly when it is oriented parallel to the loading axis.

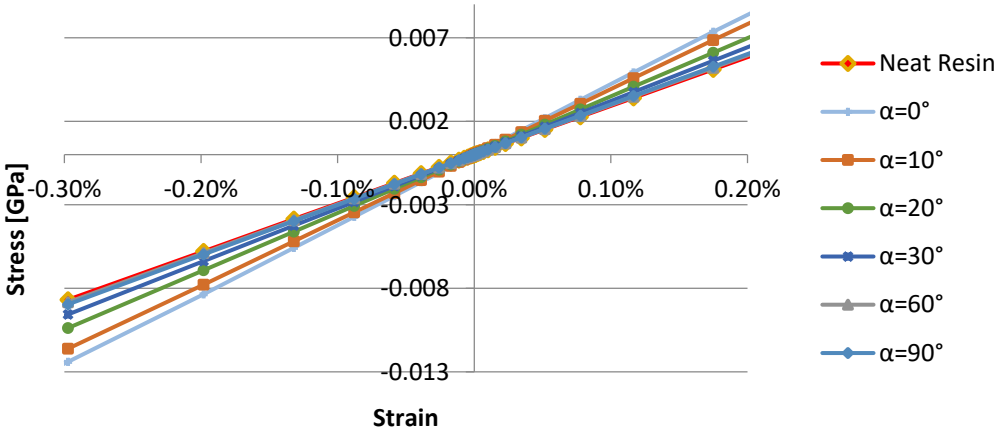

Figure 8. Tension and compression law behavior.

From Figure 9 the longitudinal Young's modulus of the composite is the highest when the CNT is aligned parallel to the loading direction, which is coherent with what is shown in Figure 10. Increasing α comes with a decrease in the stiffness up to a plateau value (reached at $\alpha = 40°$).

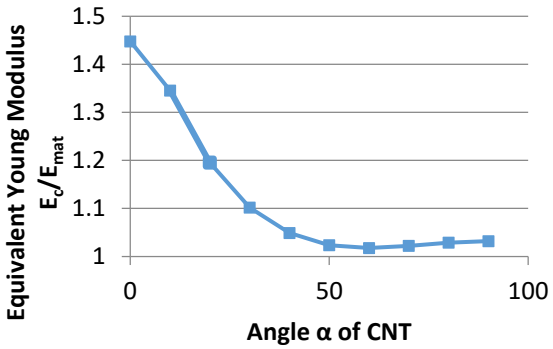

Figure 9. Evolution of the composite Young's modulus (E_c) vs. CNT orientation.

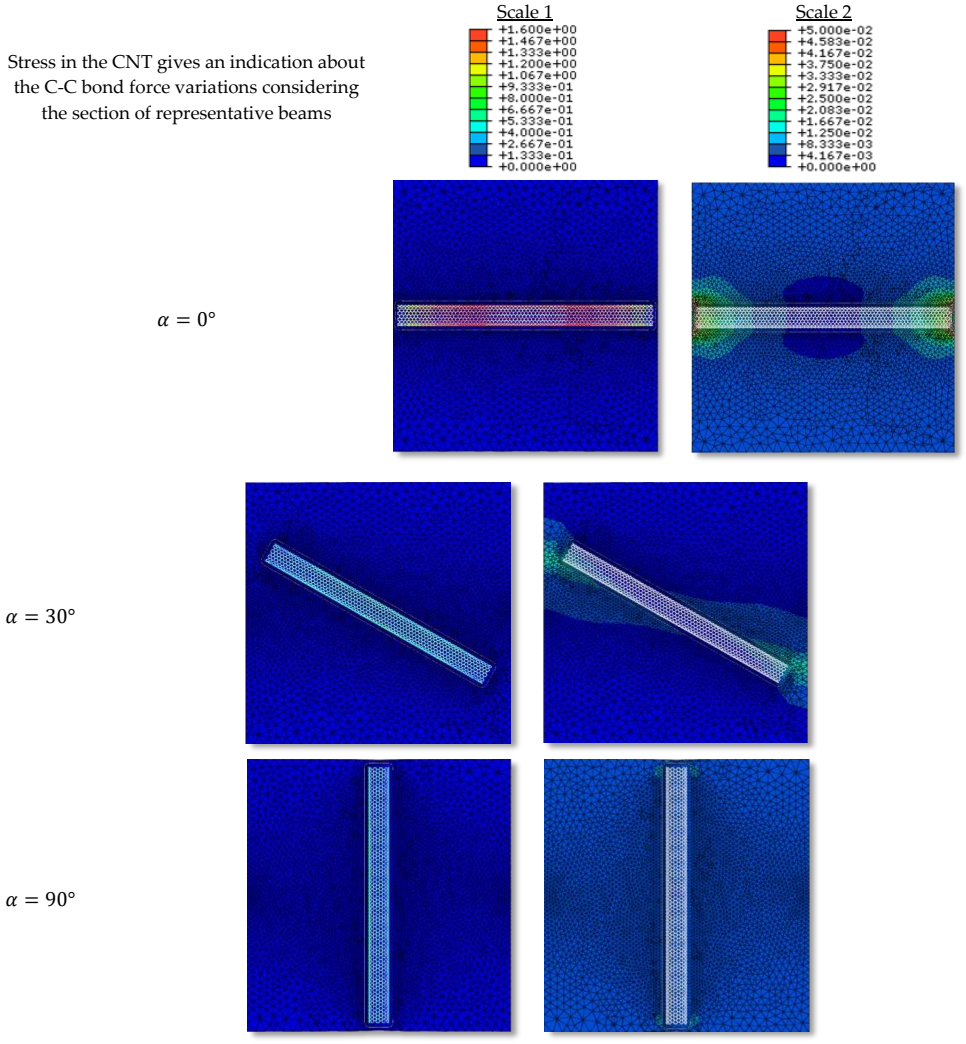

Figure 10. Illustration of the failure criteria used (Von Mises) in the CNT (left: scale 1) and the matrix (right: scale 2) in various CNT orientations, α. The same compression strain applies for all cases ($\varepsilon_{33} = -0.12\%$).

7.3. Torsion

Shear behavior has been studied by way of torsion (Figure 7). A twist angle Φ loads one end of the composite cylinder, while the second is kept fixed. Knowing that J is the polar moment of inertia, G_c is the composite shear modulus, and L is the cylinder length, the torque T is calculated as:

$$T = JG_c\frac{\Phi}{L} \tag{11}$$

As depicted in Figure 11, torsion curves are fairly similar to those of neat polymers. From Figure 12, it is clear that the CNT does not highly oppose the torsion when oriented parallel to the torsion axis. The shear modulus is the highest when $\alpha = 45°$ and when the stress is the highest.

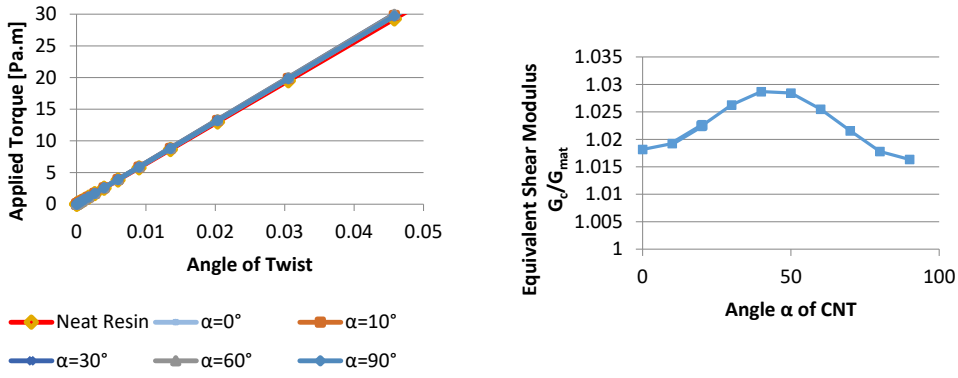

Figure 11. Left: variation of the torque vs. Φ for various values of α. Right: shear modulus G_c vs. α.

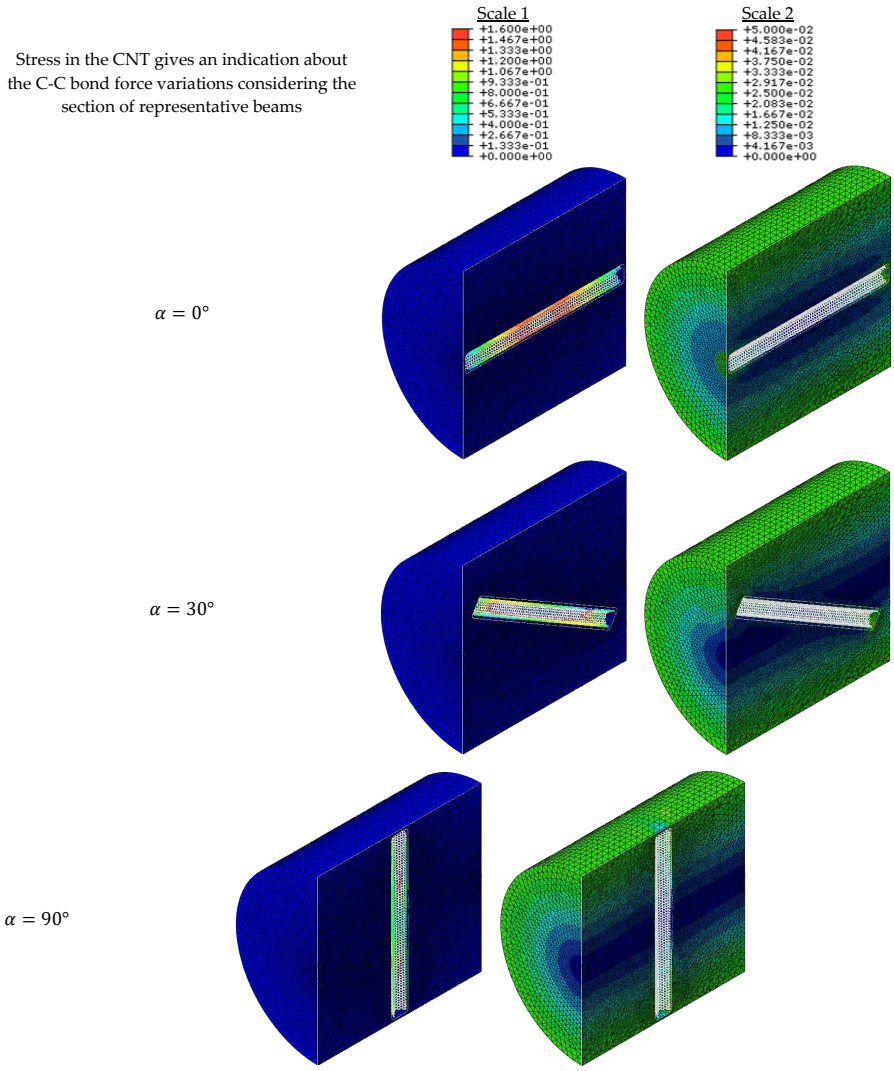

Figure 12. Von Mises Stress in the CNT (left: scale 1) and the matrix (right: scale 2) for various α. The same twist angle applies to all cases ($\Phi \approx 2°$).

7.4. Shear Test

To gain insight into the reinforcement of a bonding layer when shear-loaded, FE simulations were conducted by varying CNT orientation (Figures 13 and 14).

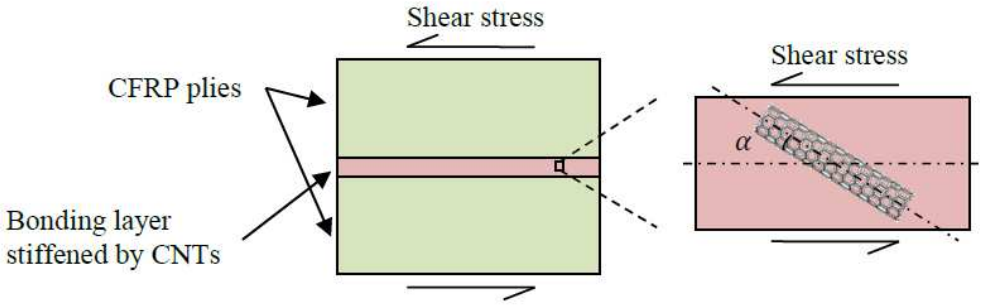

Figure 13. Illustration of the matrix layer reinforced with a CNT, which is loaded under shear.

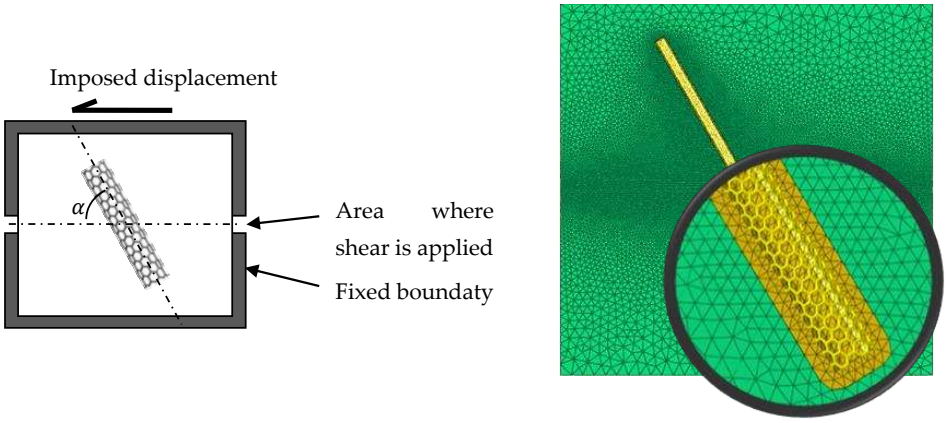

(**a**) (**b**)

Figure 14. Loading under shear: (**a**) boundary conditions; (**b**) mesh cross-section at $\alpha = 60°$.

This simulation of shear in the bonding layer is far from being straightforward since a cuboid region of matrix with a carbon nanotube, which was shear-loaded, was considered and three virtual spots within this region were defined [4] too (Figure 14).

Figure 15 shows the load applied to the block upper area vs. displacement. Once the RVE undergoes shear, nanoreinforcement is active and the RVE will show non-linear deformation, as observed when comparing neat resin vs. CNT-reinforced resin behaviors.

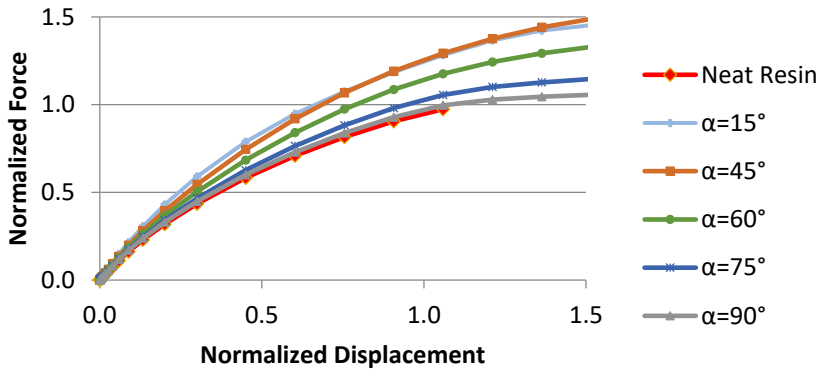

Figure 15. Force weighed to the maximal force of the neat matrix as a function of the displacement of the upper block weighed to the thickness of the middle layer.

It can also be seen in Figure 16 that reinforcement is much more important when $\alpha \in [10°, 50°]$, which can be easily understandable when considering that pressures that apply during manufacturing would surely result in CNT orientation that fall into this range.

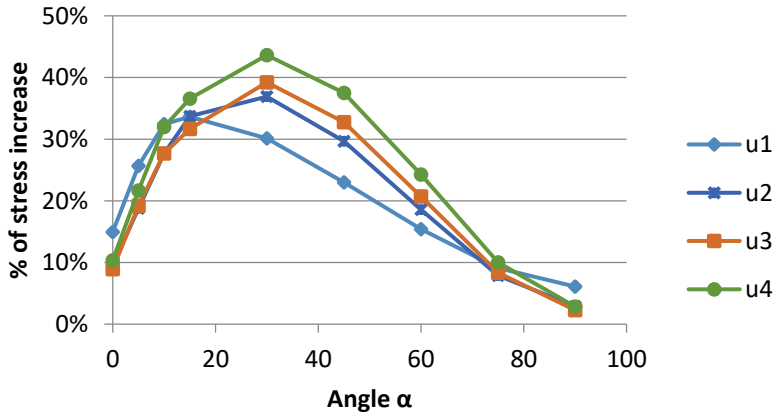

Figure 16. Increase in the shear stress for various α at various levels of displacement: $u1 = 3 \times 10^{-4}$, $u2 = 0.6$, $u3 = 1.0$ and $u4 = 1.2$

The carbon nanotube reinforces the polymer by switching the load partly from the top area to the bottom one (Figure 17), thus postponing the midsection from meeting the maximum stress.

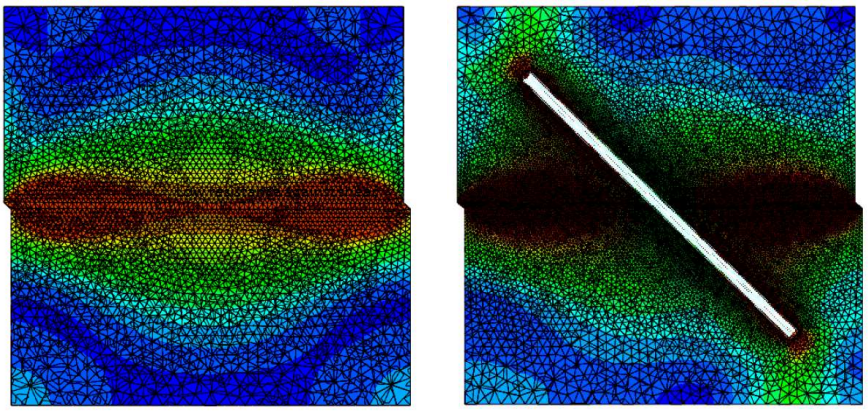

Figure 17. All matrix sections are under maximum stress (left). For the nanocomposite where $\alpha = 45°$, CNT opposes, thus delaying the maximum stress to apply at the mid-section.

Due to the high resistance of carbon-carbon bonding, CNT reinforcement is more effective when α is 45°, whereas for orientations lower than 15°, CNT–polymer interface is solely resisting shear and as a matter of fact the resistance sharply drops (Figure 17). It is worthwhile noting that if we can set the orientation to $\pm 45°$, delamination strength would be significantly improved when tension, shear and torsion apply (Figure 18).

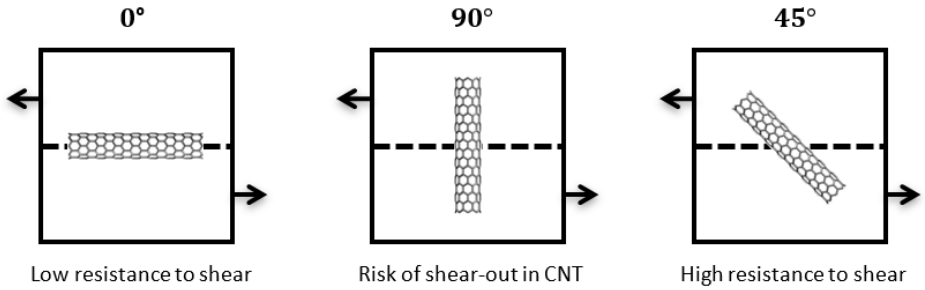

Figure 18. Illustration of the most favorable orientations of the CNT in the matrix.

7.5. Macroscopic Stiffness Tensor of the Nanocell

Homogenization was conducted to gain deep insight the linear elastic behavior of the nanocell. This was carried out using a CNT which is linear and long enough for reinforcement. The elastic stiffness tensor was numerically estimated, based on a cuboid RVE (Figure 4a) and FE modeling. A displacement $\boldsymbol{u}$, in line with a macroscopic strain $\overline{\boldsymbol{\varepsilon}}$, was applied to RVE extremities (Figure 19): $\boldsymbol{u} = \overline{\boldsymbol{\varepsilon}}.\boldsymbol{x}$, where $\boldsymbol{x}$ is the boundary point coordinate. The macroscopic stiffness tensor was calculated by considering loadings under tension ($\overline{\boldsymbol{\varepsilon}} = \boldsymbol{e_i} \otimes \boldsymbol{e_i}$, $i \in \{1,2,3\}$) and under shear ($\overline{\boldsymbol{\varepsilon}} = \boldsymbol{e_i} \otimes^s \boldsymbol{e_j}, i,\ j \in \{1,2,3\},\ i \neq j$) of the RVE boundary, $\partial\Omega$.

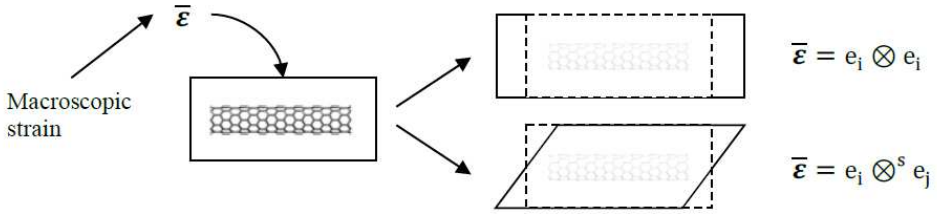

Figure 19. Illustration of the RVE considered in the tensor of stiffness.

To lower the effect of the CNT length as much as possible, a high aspect ratio was adopted along with a length equal to the RVE one. Considering an armchair (6,6) of the CNT and that the RVE is isotropic in the transverse direction (Figure 20), the tensor of compliance, $\mathbb{S}$, is given by:

$$\mathbb{S} = \begin{bmatrix} \frac{1}{E_1} & -\frac{\nu_{12}}{E_1} & -\frac{\nu_{13}}{E_1} & 0 & 0 & 0 \\ -\frac{\nu_{12}}{E_1} & \frac{1}{E_1} & -\frac{\nu_{13}}{E_1} & 0 & 0 & 0 \\ -\frac{\nu_{13}}{E_1} & -\frac{\nu_{13}}{E_1} & \frac{1}{E_3} & 0 & 0 & 0 \\ 0 & 0 & 0 & \frac{1}{2G_{13}} & 0 & 0 \\ 0 & 0 & 0 & 0 & \frac{1}{2G_{13}} & 0 \\ 0 & 0 & 0 & 0 & 0 & \frac{1+\nu_{12}}{E_1} \end{bmatrix} \quad (12)$$

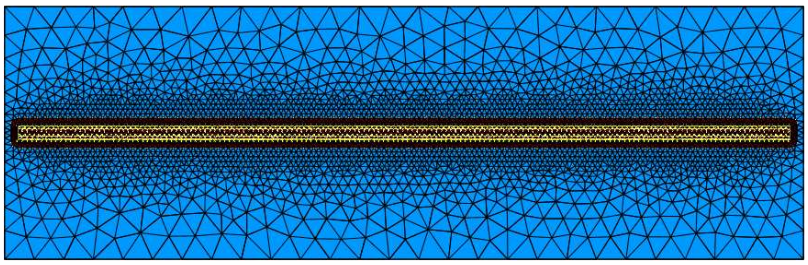

Figure 20. Illustration of the longitudinal section of the mesh of the RVE.

The macrostiffness tensor, $\mathbb{C}$, was tabulated from Equation (10) by way of compressive tests in the three directions, as well as shear loads in three plans:

$$\mathbb{C} = \mathbb{S}^{-1} = \begin{bmatrix} 6.32 & 4.21 & 4.18 & 0 & 0 & 0 \\ 4.21 & 6.32 & 4.18 & 0 & 0 & 0 \\ 4.18 & 4.18 & 9.00 & 0 & 0 & 0 \\ 0 & 0 & 0 & 2.11 & 0 & 0 \\ 0 & 0 & 0 & 0 & 2.11 & 0 \\ 0 & 0 & 0 & 0 & 0 & 2.12 \end{bmatrix} \quad (13)$$

The composite macroscopic elastic parameters are tabulated from Equations (12) and (13). Table 1 shows the comparative results for neat polymer vs. the composite. This comparison shows a high increase in the Young's modulus parallel to the CNT axis, a slight increase in transverse modulus and almost no improvement in the shear modulus.

Table 1. Elastic properties of the neat and reinforced polymer matrix.

	E_1 (GPa)	E_3 (GPa)	ν_{12}	ν_{13}	G_{13} (GPa)	G_{12} (GPa)
Neat Matrix	2.92	2.92	0.4	0.4	1.04	1.04
CNT-reinforced matrix	3.21	5.67	0.52	0.22	1.06	1.06
Ratio	1.10	1.94	-	-	1.01	1.01

8. Synthesis and Discussions

Reinforcement by CNTs can effectively enhance composite resistance under various loading axes, provided that their orientations can be mastered. It was shown that an orientation at 45° can constitute a smart "deal" that can allow a high bond strength to be achieved. It is also critical to keep in mind that the aspect ratio of the CNTs is of prime importance. When considering a CNT with a length that can be available industrially, the homogenization calculation shows a higher Young's modulus can be obtained vs. neat polymer matrices under tension and torsion, though in the case of torsion one should keep in mind that the distance to the torsion axis still influences the results (Figure 21).

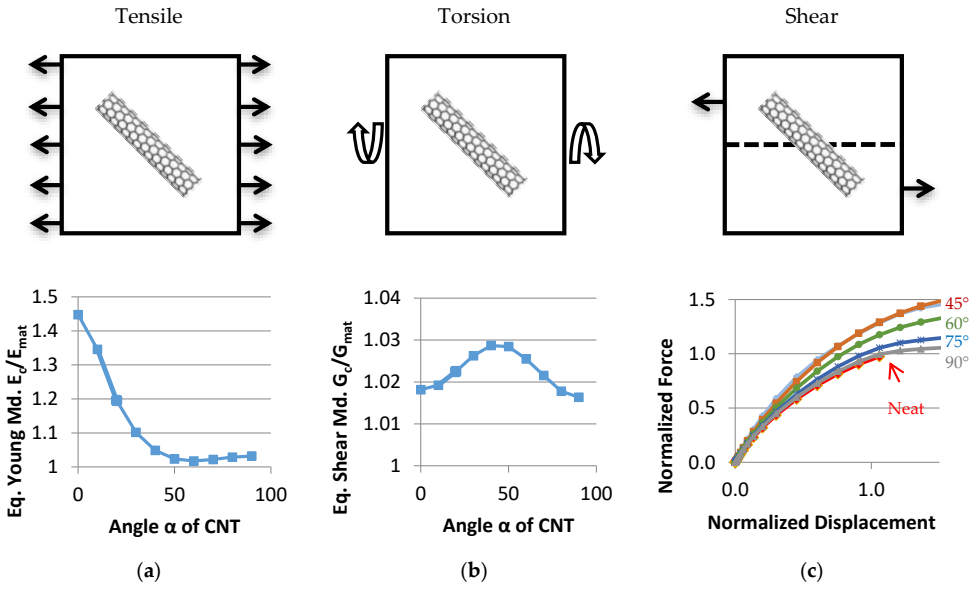

Figure 21. Summary of the simulations for tension (**a**), torsion (**b**) and shear (**c**).

9. Observations about Engineering Use

CNTs can significantly strengthen composite inter-layers or bond two composite parts. To figure out how we can make use industrially of these simulations, three-point flexure tests were numerically carried out to serve as a basis of discussion. When carbon nanotube-reinforced resin was added to the inter-layers, there was a slight increase in composite thickness vs. the case where there is no addition. In the following, we use the percent increase in both elastic moduli and shear strength, as calculated earlier.

The composite under focus is made of 12 plies of CFRP oriented at $0°$, $45°$ and $-45°$. Carbon nanotube-reinforced resin was added in the inter-plies. Models that were used are based on ASTM D7264/D7264M [52] (Figure 22). The ply thickness is 0.33 mm, that of the CNT-reinforced layer is 0.20 mm, whole composite thickness is 6.2 mm, an aspect ratio of 1/16 was selected, the span is 98.6 mm, the total specimen length is 118 mm and the width is 13.0 mm. Abaqus was used for simulations, the layers were continuum shells, and mesh was refined in the areas close to supports and at the center, while they were made coarser in all other areas, as shown in Figure 23.

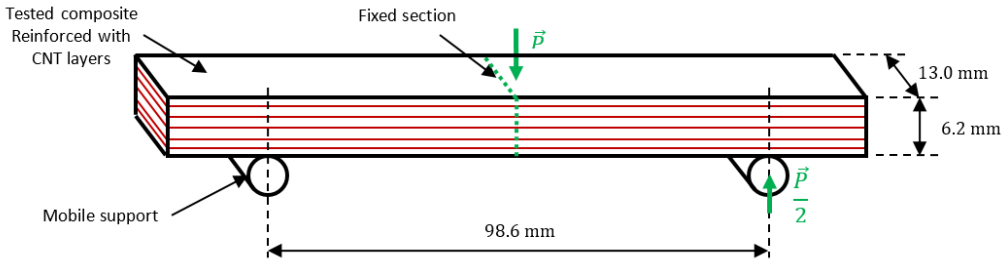

Figure 22. Illustration of 3-point bend test.

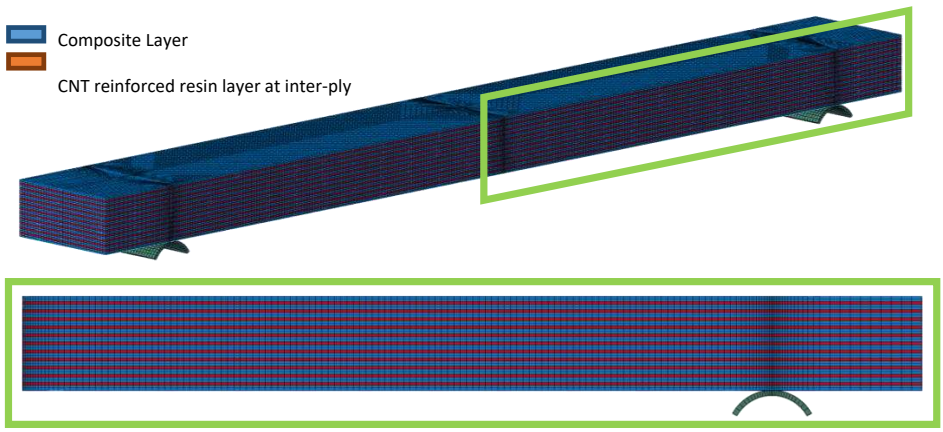

Figure 23. Illustration of the mesh of the simulated half-specimen.

The CFRPs that were considered are made of 60% of AS4 fibers and 40% of 3501-6 epoxy [53]. To account for CNT reinforcement, an average increase of 60% of elastic modulus was considered, as well 30% of shear strength. Material parameters are listed in Table 2.

Table 2. Summary of the elastic parameters considered in the study.

	E_1 (GPa)	E_3 (GPa)	ν_{12}	G_{12} (GPa)	G_{13} (GPa)	G_{23} (GPa)
CFRP ply (tension)	141	11	0.28	6.6	4.8	4.8
CFRP ply (compression)	128	11	0.28	6.6	4.8	4.8
Reinforced resin in inter-ply	6.7		0.4		1.6	

Damage initiation was predicted using the Hashin criterion [54,55]. Accordingly, tension and compression strength were parallel to the fiber axis (named direction 1), tension and compression strength were perpendicular to the fiber axis (named direction 2) and longitudinal and transverse shear strengths. Material properties are listed in Table 3.

Table 3. Illustration of the limits of elasticity considered in the study.

		Plies (MPa)	CNT Reinforced Resin (MPa)
Compression strength-direction 1	X_c	1950	300
Compression strength-direction 2	Y_c	200	
Tension strength-direction 1	X_t	1950	82
Tension strength-direction 2	Y_t	81	
Shear strength	S_l	79	67
Transverse shear strength	S_t	79	

In the case of flexure, damage starts at the maximum deflection point and then propagates through the section. Compressive damage takes place at the top of the specimen following the penetration of the central span into the material. Thereafter, multiple delamination takes place at the inter-plies. Delamination is easily initiated when the inter-plis shear strength is weak. It is therefore easily understandable that increasing the interply strength through the use of CNT-reinforced resin will surely lead to the increase in the composite's Young's modulus.

A vertical load was applied to the center of the specimen. Rigid and frictionless cylinders with diameters of 6mm were considered according to the standards. Side displacement was not allowed. The considered composite architecture was unidirectional $[0°]^{6S}$ and 2D $[45°/-45°]^{3S}$.

9.1. Unidirectional Specimen [0°]

Figure 24 shows the load vs. deflection. As expected, damage initiates at the fibers located at the lower surface of the specimen. Note that damage initiated at 1 kN for the unreinforced composite, whereas this value jumped to 1.6 kN in the CNT-reinforced composite (Figure 24), which represents a 60% increase.

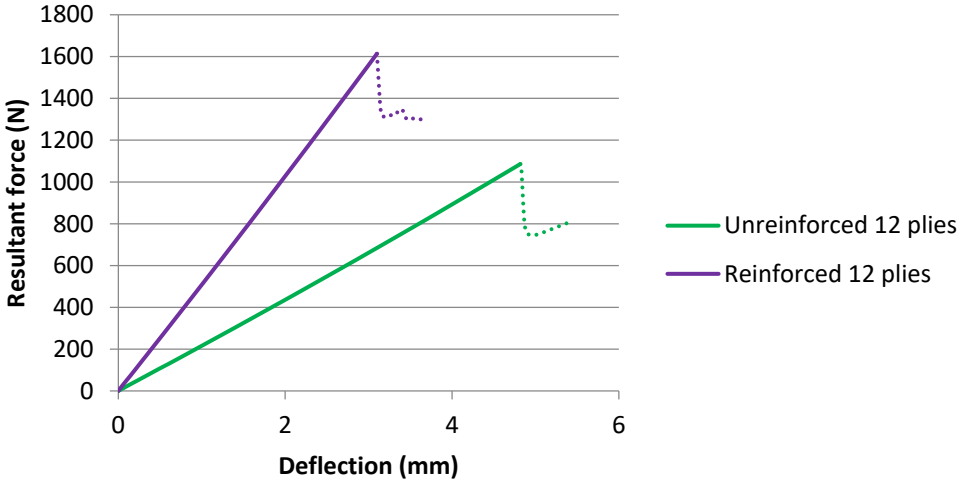

Figure 24. Load–displacement and stiffness comparison before damage in 0° plies (case 1).

The test shows significant improvement in stiffness, which results from the section-quadratic moment. It is therefore clear that CNT addition at the inter-plies comes with an increase in the composite stiffness. Its resistance to delamination is improved as well.

9.2. 2-Dimensional Specimen [45°]

The elastic modulus is lower than in UD. Figure 25 shows the load–displacement curve that highlights very similar results. Damage initiates in the matrix at the lower surface. Additionally, there is a clear increase in stiffness and damage is delayed in CNT-reinforced specimens.

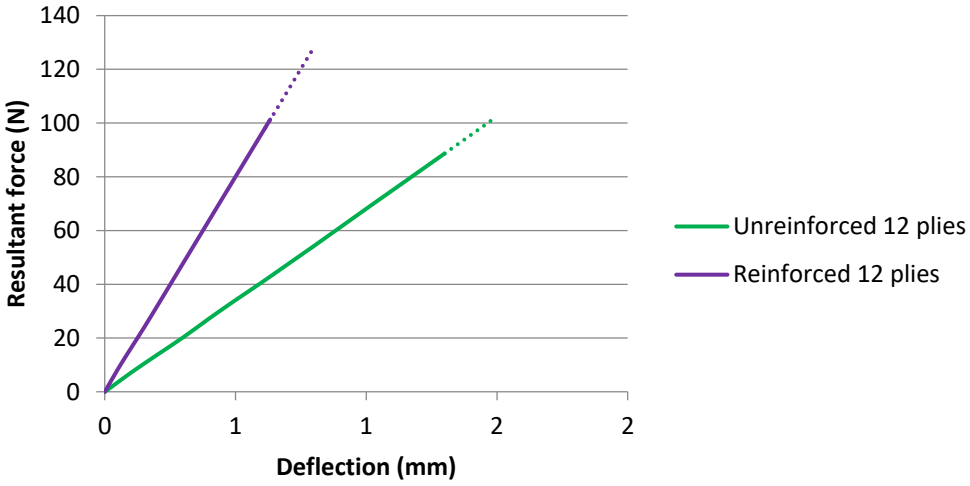

Figure 25. Load–displacement and stiffness comparison before damage in $+45°/-45°$ (case 2).

To sum up, numerical bending tests, which were carried out taking into account industrial constraints (in particular the size of the carbon nanotubes and the thickness gradient of the composite plies following the addition of a reinforced matrix overlay by CNTs) have shown that stiffness is improved, as well as the resistance to delamination. It goes without saying that future work should include several additional variables to support the current work. For example, it would be interesting to work further by including hygro-thermal effects, using the approaches of [56–58], for example.

10. Prospective

This study was conducted considering the ideal case of a nanometric cell represented by a matrix reinforced by a single carbon nanotube. The study was carried out in a

case where the carbon nanotubes were homogeneously dispersed within a resin and were functionalized and that their achieved orientations were ideal and at an industrial scale. In reality, we are still a long way from this case and the difficulties should be well foreshadowed. First of all, obtaining a significant dispersion of the nanotubes is very difficult as, despite all the precautions that one takes, this operation remains eminently delicate. Indeed, not only the mixture must disperse the nanotubes, but it is also necessary to be careful not to degrade them. Let us also keep in mind that the state of the dispersion depends on the scale and the area (or volume) studied and this easily suggests the extent of the difficulty when dealing with large quantities of resins. The orientation of the carbon nanotubes is also a major disturbance as although this is relatively easy in the case of short fibers, the operation is very complicated for nanometric particles. All this obliges us to remain very humble and to keep thinking and work hard in order to improve our understanding of the mechanisms involved, while proposing scenarios for solving the issues encountered to best benefit the reinforcement of composite structures using carbon nanotubes.

11. Further Thinking

The proposed research is also part of a deep theoretical rethinking of the reinforcement mechanisms operating at different scales (nano to macro) and their kinetic of operating. Indeed, the reinforcement of composites is a set of mechanisms which operate at different scales (from nano to macro) and implies for each scale the net type and the size of the reinforcement specific to the considered scale. Therefore, the question that arises is whether the reinforcement at a given scale ceases to operate or not once we go up to the next scale, knowing that the best scenario would obviously be that all the reinforcements can develop continuously their benefits at any scale, under any loading configuration and at any loading speed. Figure 26 is illustrating the modeling pathway that takes researchers and engineers from the nanoscale all the way towards the final structure as suggested by Drissi-Habti [59]. Beyond a numerical modeling which can always be undertaken in a rigorous way, by using available theoretical and mathematical arsenals, the question will be asked whether physically the composite reinforced either with CNTs and continuous fibers, subjected to a stress scenario will be able to oppose these constraints efficiently by concomitant use of all the reinforcements available. In the same vein, if this is not the case, what are the options that would be worthwhile to test.

On the basis of the results presented along with a deep step-back thinking, it seems rather improbable, if not impossible, that the composite whose matrix is reinforced by carbon nanotubes, on one hand, and continuous fibers, on the other hand, could benefit fully from nanometric reinforcement. The reason for this lies in the fact that there is no physical continuity between carbon nanotubes and fibers and/or fiber fabrics. We consider that reinforcement of matrices can only be efficient if its overall architecture is responding as one and only one entity. In other words, an efficient technological reinforcement solution for all scales could only be seen if we manage to develop an "all-in-one" reinforcement—for example, 2D fabrics and/or multi-D based on a continuous fiber having a surface crimped by carbon nanotubes of length "enough long" (Figure 27). The *physical continuity* of such CNT reinforcement to fiber to cloth to the macrocomposite would give guarantees of performance such as those demanded by the critical underlying industries. Obviously, the idea presented remains a preliminary concept that must be studied from scratch by optimizing all stages.

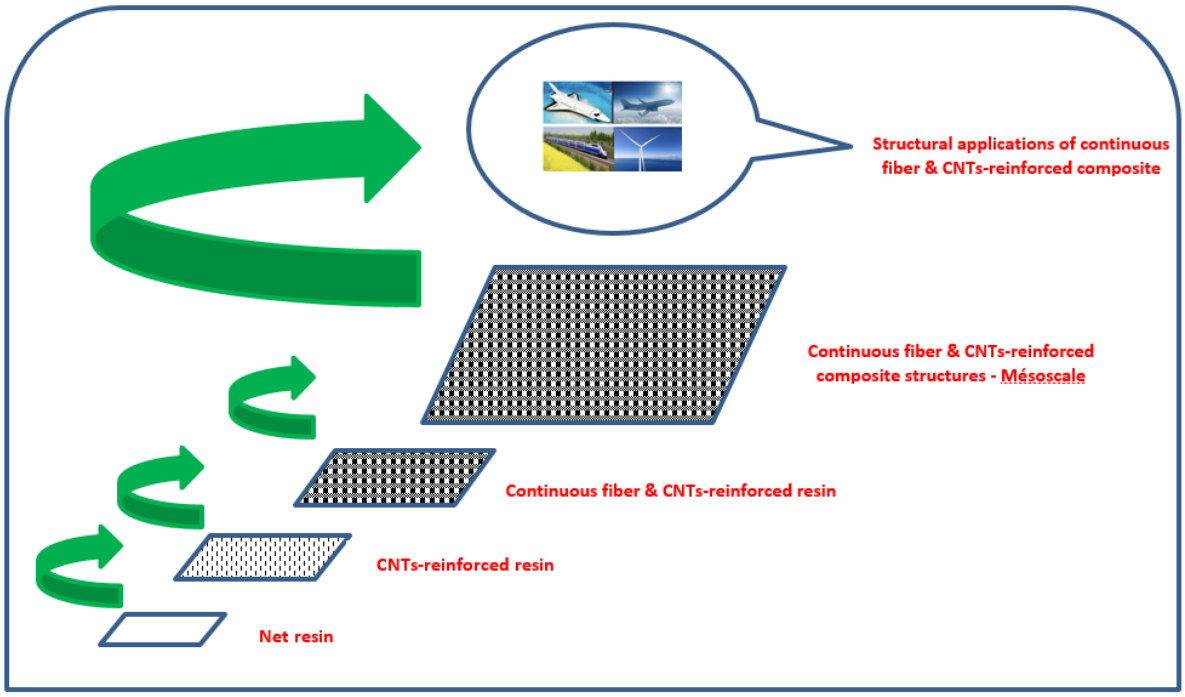

Figure 26. Illustration of the pathway of modeling from nano to macro of smart composite reinforced by continuous fibers and carbon nanotubes.

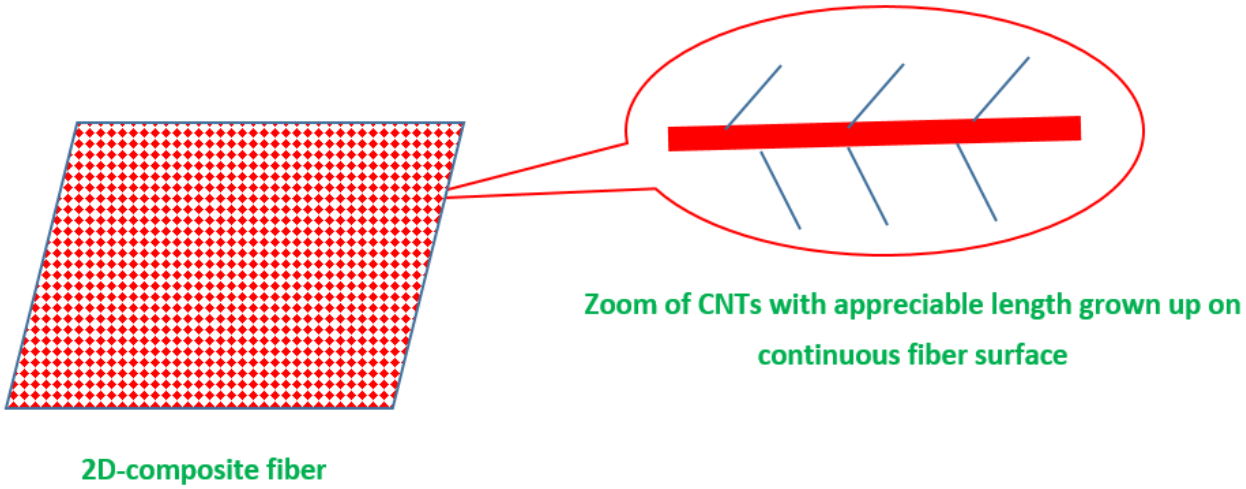

Figure 27. Illustration of the suggested "continuous" reinforcement that is made of continuous fiber with CNTs of "enough" length grown up on their surfaces, which were then woven before adding the matrix.

12. Conclusions

FE modeling was carried out to investigate CNT reinforcement to improve mechanical properties of CFRPs inter-ply areas and bond joints strength as well. The article targeted the increase in composite delamination strength, which is a critical property for composites. The models are expected to bring innovative solutions for reinforcing bonding joints of large structures that are used in aggressive environments, such as offshore wind-blades of lengths exceeding 100m.

Numerical homogenization was performed to calculate the macroscopic mechanical properties of composite structures based on the RVE models. It was shown that mastering the orientation of carbon nanotubes is the key to achieving the best mechanical properties.

If future technologies allow controlling CNT orientations, large and very high performance composite parts can be fabricated.

The development of an "all-in-one" reinforcement ensuring physical continuity between carbon nanotubes and the continuous fiber can be an efficient technological reinforcement solution, as in the example of 2D fabrics based on a continuous fiber having a surface crimped with carbon nanotubes of "long enough" lengths. The physical continuity of such a reinforcement from the nanoscale to macroscale would give guarantees of performances for advanced industries, provided that this concept is implemented from scratch, and can be strengthened by deep modeling and optimization of various parameters involved.

Author Contributions: M.D.-H. worked on the basic concept of the models, their contours and the organization of the results. Y.E.A. designed the models and made the calculations under the supervision of M.D.-H. V.R. provided support in numerical modeling under the supervision of M.D.-H. All authors have read and agreed to the published version of the manuscript.

Funding: This research received no external funding.

Acknowledgments: M.D.-H. would like to thank the French National Research Agency (ANR) for the support of this research (French–German ANR-BMBF Contract REHSTRAIN).

Conflicts of Interest: The authors declare no conflict of interest.

References

1. Drissi-Habti, M.; Raman, V.; Khadour, A.; Timorian, S. Fiber Optic Sensor Embedment Study for Multi-Parameter Strain Sensing. *Sensors* **2017**, *17*, 667. [CrossRef] [PubMed]
2. Raman, V.; Drissi-Habti, M. Numerical simulation analysis as a tool to identify areas of weakness in a turbine wind-blade and solutions for their reinforcement. *Compos. Part B* **2016**, *103*, 23–39. [CrossRef]
3. Raman, V.; Drissi-Habti, M. Numerical simulation of a resistant structural bonding in wind-turbine blade through the use of composite cord stitching. *Compos. Part B Eng.* **2019**, *176*, 107094. [CrossRef]
4. El-Assami, Y.; Drissi-Habti, M. Stiffening offshore composite wind-blades bonding joints by carbon nanotubes reinforced resin–a new concept. *J. Struct. Integr. Maint.* **2020**, *5*, 87–103. [CrossRef]
5. Thostenson, E.T.; Ren, Z.; Chou, T.-W. Advances in the science and technology of carbon nanotubes and their composites: A review. *Compos. Sci. Technol.* **2001**, *61*, 1899–1912. [CrossRef]
6. Ruoff, R.S.; Qian, D.; Liu, W.K. Mechanical properties of carbon nanotubes: Theoretical predictions and experimental measurements. *Comptes Rendus Phys.* **2003**, *4*, 993–1008. [CrossRef]
7. Meo, M.; Rossi, M. Prediction of Young's modulus of single wall carbon nanotubes by molecular-mechanics based finite element modelling. *Compos. Sci. Technol.* **2006**, *66*, 1597–1605. [CrossRef]
8. Tserpes, K.I.; Papanikos, P.; Tsirkas, S.A. A progressive fracture model for carbon nanotubes. *Compos. Part B Eng.* **2006**, *37*, 662–669. [CrossRef]
9. Gou, J.; Lau, K. Modeling and Simulation of Carbon Nanotube/Polymer Composites. In *Handbook of Theoretical and Computational Nanotechnology*; American Scientific Publisher: New Orleans, LA, USA, 2005; Volume 1, pp. 1–33.
10. Zeng, Q.H.; Yu, A.B.; Lu, G.Q. Multiscale modeling and simulation of polymer nanocomposites. *Prog. Polym. Sci.* **2008**, *33*, 191–269. [CrossRef]
11. Montazeri, A.; Montazeri, N. Viscoelastic and mechanical properties of multi walled carbon nanotube/epoxy composites with different nanotube content. *Mater. Des.* **2011**, *32*, 2301–2307. [CrossRef]
12. Mittal, G.; Dhand, V.; Rhee, K.Y.; Park, S.-J.; Lee, W.R. A review on carbon nanotubes and graphene as fillers in reinforced polymer nanocomposites. *J. Ind. Eng. Chem.* **2015**, *21*, 11–25. [CrossRef]
13. Lahiri, D.; Bakshi, S.R.; Keshri, A.K.; Liu, Y.; Agarwal, A. Dual strengthening mechanisms induced by carbon nanotubes in roll bonded aluminum composites. *Mater. Sci. Eng. A* **2009**, *523*, 263–270. [CrossRef]
14. Rousakis, T.C.; Kouravelou, K.B.; Karachalios, T.K. Effects of carbon nanotube enrichment of epoxy resins on hybrid FRP–FR confinement of concrete. *Compos. Part B Eng.* **2014**, *57*, 210–218. [CrossRef]
15. Dong, S.; Zhou, J.; Hui, D.; Wang, Y.; Zhang, S. Size dependent strengthening mechanisms in carbon nanotube reinforced metal matrix composites. *Compos. Part Appl. Sci. Manuf.* **2015**, *68*, 356–364. [CrossRef]
16. Sinnott, S.B.; Andrews, R. Carbon Nanotubes: Synthesis, Properties, and Applications. *Crit. Rev. Solid State Mater. Sci.* **2001**, *26*, 145–249. [CrossRef]
17. Bellucci, S. Carbon nanotubes: Physics and applications. *Phys. Status Solidi C* **2005**, *2*, 34–47. [CrossRef]
18. Vahedi, F.; Shahverdi, H.R.; Shokrieh, M.M.; Esmkhani, M. Effects of carbon nanotube content on the mechanical and electrical properties of epoxy-based composites. *New Carbon Mater.* **2014**, *29*, 419–442. [CrossRef]
19. Sinnott, S.B.; Shenderova, O.A.; White, C.T.; Brenner, D.W. Mechanical properties of nanotubule fibers and composites determined from theoretical calculations and simulations. *Carbon* **1998**, *36*, 1–9. [CrossRef]

20. Mao, Z.; Garg, A.; Sinnott, S.B. Molecular dynamics simulations of the filling and decorating of carbon nanotubules. *Nanotechnology* **1999**, *10*, 273. [CrossRef]
21. Odegard, G.M.; Gates, T.S.; Wise, K.E.; Park, C.; Siochi, E.J. Constitutive modeling of nanotube–reinforced polymer composites. *Compos. Sci. Technol.* **2003**, *63*, 1671–1687. [CrossRef]
22. Zuberi, M.J.S.; Esat, V. Investigating the mechanical properties of single walled carbon nanotube reinforced epoxy composite through finite element modelling. *Compos. Part B Eng.* **2015**, *71*, 1–9. [CrossRef]
23. Liu, Y.H.B. The atomic-scale finite element method. *Comput. Methods Appl. Mech. Eng.* **2004**, *193*, 1849–1864. [CrossRef]
24. Liu, H.J.B. Atomic-scale finite element method in multiscale computation with applications to carbon nanotubes. *Phys. Rev. B* **2005**, *72*. [CrossRef]
25. Leung, A.Y.T.; Guo, X.; He, X.Q.; Jiang, H.; Huang, Y. Postbuckling of carbon nanotubes by atomic-scale finite element. *J. Appl. Phys.* **2006**, *99*, 124308. [CrossRef]
26. Odegard, G.M.; Gates, T.S.; Nicholson, L.M.; Wise, K.E. Equivalent-continuum modeling of nano-structured materials. *Compos. Sci. Technol.* **2002**, *62*, 1869–1880. [CrossRef]
27. Li, C.; Chou, T.-W. A structural mechanics approach for the analysis of carbon nanotubes. *Int. J. Solids Struct.* **2003**, *40*, 2487–2499. [CrossRef]
28. Li, C.; Chou, T.-W. Multiscale Modeling of Carbon Nanotube Reinforced Polymer Composites. *J. Nanosci. Nanotechnol.* **2003**, *3*, 423–430. [CrossRef]
29. Lu, X.; Hu, Z. Mechanical property evaluation of single-walled carbon nanotubes by finite element modeling. *Compos. Part B Eng.* **2012**, *43*, 1902–1913. [CrossRef]
30. Li, C.; Chou, T.-W. Elastic moduli of multi-walled carbon nanotubes and the effect of van der Waals forces. *Compos. Sci. Technol.* **2003**, *63*, 1517–1524. [CrossRef]
31. Li, C.; Chou, T.-W. Multiscale modeling of compressive behavior of carbon nanotube/polymer composites. *Compos. Sci. Technol.* **2006**, *66*, 2409–2414. [CrossRef]
32. Gojny, F.H.; Wichmann, M.H.G.; Fiedler, B.; Schulte, K. Influence of different carbon nanotubes on the mechanical properties of epoxy matrix composites–A comparative study. *Compos. Sci. Technol.* **2005**, *65*, 2300–2313. [CrossRef]
33. Fiedler, B.; Gojny, F.H.; Wichmann, M.H.G.; Nolte, M.C.M.; Schulte, K. Fundamental aspects of nano-reinforced composites. *Compos. Sci. Technol.* **2006**, *66*, 3115–3125. [CrossRef]
34. Jeon, I.-Y.; Chang, D.W.; Kumar, N.A.; Baek, J.-B. Functionalization of Carbon Nanotubes. In *Carbon Nanotubes-Polymer Nanocomposites*; Intech: London, UK, 2011.
35. Gojny, F.H.; Schulte, K. Functionalisation effect on the thermo-mechanical behaviour of multi-wall carbon nanotube/epoxy-composites. *Compos. Sci. Technol.* **2004**, *64*, 2303–2308. [CrossRef]
36. Yang, Y.-B.; Shieh, M.-S. Solution method for nonlinear problems with multiple critical points. *AIAA J.* **1990**, *28*, 2110–2116. [CrossRef]
37. Gupta, A.K.; Harsha, S.P. Analysis of mechanical properties of carbon nanotube reinforced polymer composites using multi-scale finite element modeling approach. *Compos. Part B Eng.* **2016**, *95*, 172–178. [CrossRef]
38. Jiang, L.Y.; Huang, Y.; Jiang, H.; Ravichandran, G.; Gao, H.; Hwang, K.C.; Liu, B. A cohesive law for carbon nanotube/polymer interfaces based on the van der Waals force. *J. Mech. Phys. Solids* **2006**, *54*, 2436–2452. [CrossRef]
39. He, X.Q.; Kitipornchai, S.; Wang, C.M.; Liew, K.M. Modeling of van der Waals force for infinitesimal deformation of multi-walled carbon nanotubes treated as cylindrical shells. *Int. J. Solids Struct.* **2005**, *42*, 6032–6047. [CrossRef]
40. Esbati, A.; Irani, S. Mechanical properties and fracture analysis of functionalized carbon nanotube embedded by polymer matrix. *Aerosp. Sci. Technol.* **2016**, *55*, 120–130. [CrossRef]
41. Liu, X.; Yang, Q.-S.; He, X.-Q.; Liew, K.-M. Cohesive laws for van der Waals interactions of super carbon nanotube/polymer composites. *Mech. Res. Commun.* **2016**, *72*, 33–40. [CrossRef]
42. Namilae, S.; Chandra, N. Multiscale Model to Study the Effect of Interfaces in Carbon Nanotube-Based Composites. *J. Eng. Mater. Technol.* **2005**, *127*, 222–232. [CrossRef]
43. Qian, D.; Dickey, E.C.; Andrews, R.; Rantell, T. Load transfer and deformation mechanisms in carbon nanotube-polystyrene composites. *Appl. Phys. Lett.* **2000**, *76*, 2868–2870. [CrossRef]
44. Brenner, D.W.; Shenderova, O.A.; Harrison, J.A.; Stuart, S.J.; Ni, B.; Sinnott, S.B. A second-generation reactive empirical bond order (REBO) potential energy expression for hydrocarbons. *J. Phys. Condens. Matter* **2002**, *14*, 783. [CrossRef]
45. Gao, X.-L.; Li, K. A shear-lag model for carbon nanotube-reinforced polymer composites. *Int. J. Solids Struct.* **2005**, *42*, 1649–1667. [CrossRef]
46. Chang, T.; Gao, H. Size-dependent elastic properties of a single-walled carbon nanotube via a molecular mechanics model. *J. Mech. Phys. Solids* **2003**, *51*, 1059–1074. [CrossRef]
47. Tserpes, K.I.; Papanikos, P. Finite element modeling of single-walled carbon nanotubes. *Compos. Part B Eng.* **2005**, *36*, 468–477. [CrossRef]
48. Scarpa, F.; Adhikari, S. A mechanical equivalence for Poisson's ratio and thickness of C–C bonds in single wall carbon nanotubes. *J. Phys. Appl. Phys.* **2008**, *41*, 085306. [CrossRef]
49. Chen, Y.L.; Liu, B.; He, X.Q.; Huang, Y.; Hwang, K.C. Failure analysis and the optimal toughness design of carbon nanotube-reinforced composites. *Compos. Sci. Technol.* **2010**, *70*, 1360–1367. [CrossRef]

50. Littell, J.D.; Ruggeri, C.R.; Goldberg, R.K.; Roberts, G.D.; Arnold, W.A.; Binienda, W.K. Measurement of Epoxy Resin Tension, Compression, and Shear Stress–Strain Curves over a Wide Range of Strain Rates Using Small Test Specimens. *J. Aerosp. Eng.* **2008**, *21*, 162–173. [CrossRef]
51. Kumar, A.; Li, S.; Roy, S.; King, J.A.; Odegard, G.M. Fracture properties of nanographene reinforced EPON 862 thermoset polymer system. *Compos. Sci. Technol.* **2015**, *114*, 87–93. [CrossRef]
52. Liu, Q. Hill's lemma for the average-field theory of Cosserat continuum. *Acta Mech.* **2012**, *224*, 851–866. [CrossRef]
53. *Standard Test Method for Flexural Properties of Polymer Matrix Composite Materials*; ASTM International: West Conshohocken, PA, USA, 2015.
54. Soden, P.D.; Hinton, M.J.; Kaddour, A.S. Lamina properties, lay-up configurations and loading conditions for a range of fibre-reinforced composite laminates. *Compos. Sci. Technol.* **1998**, *58*, 1011–1022. [CrossRef]
55. Hashin, Z. A Fatigue Failure Criterion for Fiber Reinforced Materials. *J. Compos. Mater.* **1973**, *7*. [CrossRef]
56. Hashin, Z. Failure Criteria for Unidirectional Fiber Composites. *J. Appl. Mech.* **1980**, *47*, 329–334. [CrossRef]
57. Bisheh, H.; Wu, N. Wave propagation in smart laminated composite cylindrical shells reinforced with carbon nanotubes in hygrothermal environments. *Compos. Part B Eng.* **2019**, *162*, 219–241. [CrossRef]
58. Bisheh, H.; Wu, N.; Rabczuk, T. Free vibration analysis of smart laminated carbon nanotube-reinforced composite cylindrical shells with various boundary conditions in hygrothermal environments. *Thin-Walled Struct.* **2020**, *149*, 106500. [CrossRef]
59. Drissi-Habti, M. A new chart method for assessing the performance of ceramic matrix composites and aiding numerical modelling. *Annal. Chim. Sci. Matér.* **2000**, *25*, 551–556. [CrossRef]